New Methods for the Study of Defect Distributions in the Copper Indium Diselenide Alloys

J. David Cohen[a], Jennifer T. Heath[a], and William N. Shafarman[b]
[a]Department of Physics and Materials Science Institute, University of Oregon, Eugene, OR 97403
[b]Institute for Energy Conversion, University of Delaware, Newark, DE 19716

ABSTRACT

We have recently been successful utilizing two methods which are new to the study of CIGS thin film samples: drive-level capacitance profiling, and transient photo-capacitance spectroscopy. In this paper we review several of the key results that we have obtained by applying these methods to the study of the CIGS alloys over the past year. This has resulted not only in new information concerning the deep defects and their spatial distributions in these materials, but also to more accurate determinations of free carrier densities, of minority carrier trapping dynamics within the junction region, and of metastable deep defect creation within the absorber region.

1. Introduction

The methods of transient photocapacitance (TPC) spectroscopy and drive-level capacitance profiling (DLCP) have been applied to the study of $CuIn_{1-x}Ga_xSe_2$ (CIGS) photovoltaic sample devices fabricated at IEC. In this paper we will report some of the new information about the gap state defect distributions that has been revealed by the TPC method and how this technique can be used to deduce minority carrier collection efficiencies in these devices. We will also show how the DLCP method can be used to help distinguish defects in the bulk absorber from defects lying near the junction interface. Moreover, we will use DLCP to demonstrate that light soaking actually increases the defects in bulk absorber for these samples in a metastable fashion.

2. Sample preparation

The polycrystalline devices were fabricated at the Institute of Energy Conversion at the University of Delaware. CIGS films were grown about 2 µm thick using four-source elemental evaporation, as discussed previously [1,2]. The film compositions, determined by energy dispersive x-ray spectroscopy, are slightly Cu poor, with Cu/(In+Ga)=0.8-0.9. The films were prepared with x values ranging from 0 to 0.8, resulting in a bandgap energies, E_g, ranging from roughly 1.0 to 1.6 eV. Auger depth profiles indicate uniform Ga compositions in these samples.

The CIGS films were deposited on soda-lime glass which had been coated with a 1 µm Mo layer. In most samples, the CIGS films were grown at substrate temperatures T_{ss} = 550 °C, although a few samples were prepared with T_{ss} = 480 °C and T_{ss} = 400 °C. To form devices, chemical bath deposition was used to deposit 30-40 nm of CdS, then ZnO:Al was sputtered to form the top contact, with evaporated Ni/Al grids. Device efficiencies were typically 14-16 %, but were 11% for the lowest T_{ss} device.

3. Transient Photocapacitance Spectroscopy

Sensitive measurements of the optical absorption in semiconductors have been used to reveal two important aspects of the electronic structure associated with the bandgap: the exponential Urbach tail, and the optical transitions associated with deep defects. The former is an indicator of the disorder within a semiconductor. It also provides some insight into carrier properties since carrier hopping in and out of bandtail states usually limits their effective mobility. The deep defect absorption signal provides a way to examine defect transitions that are not observable by standard admittance spectroscopic measurements; i.e., beyond those associated with majority carrier trapping. Thus, one can also observe defect levels that may be associated with minority carrier trapping and/or recombination.

Direct optical transmission/reflectivity measurements are simply not sensitive enough to examine CIGS in its thin film form. Alternative techniques suitable for other thin film materials such as photothermal deflection spectroscopy (PDS) or the constant photocurrent method (CPM) are also unsuitable if one wants to measure films as deposited into the normal photovoltaic device configuration. Transient photocapacitance (TPC) spectroscopy, on the other hand, can be applied directly to these devices without further modification. Although initially developed for the study of amorphous silicon materials [3], this method has been found by us to be even more ideally suited to CIGS.

The principle and implementation of this method is similar to the more familiar DLTS technique. The semiconductor junction held under reverse bias is subjected periodically to a voltage filling pulse which allows majority carriers to move into the previously depleted region and be captured. Following these pulses a capacitance transient can be observed as holes are thermally emitted out of the majority carrier traps and leave the depletion region. In the TPC measurement, however, we introduce sub-band-gap monochromatic light to induce optical transitions in addition to any thermal ones. Actually, we apply light after *every other* filling pulse so that the capacitance transients with and without light present can be subtracted. The *difference* integrated over a time window and normalized to the photon flux yields the photocapacitance signal at each photon energy selected by the monochromator. Repeating this over the full range of sub-band-gap photon energies available yields the *photocapacitance spectrum*. An example of such a spectrum for a 30% Ga fraction CIGS alloy sample is displayed as the solid triangles in Fig. 1. Additional spectra for samples containing a range of Ga fractions are displayed in Fig. 2.

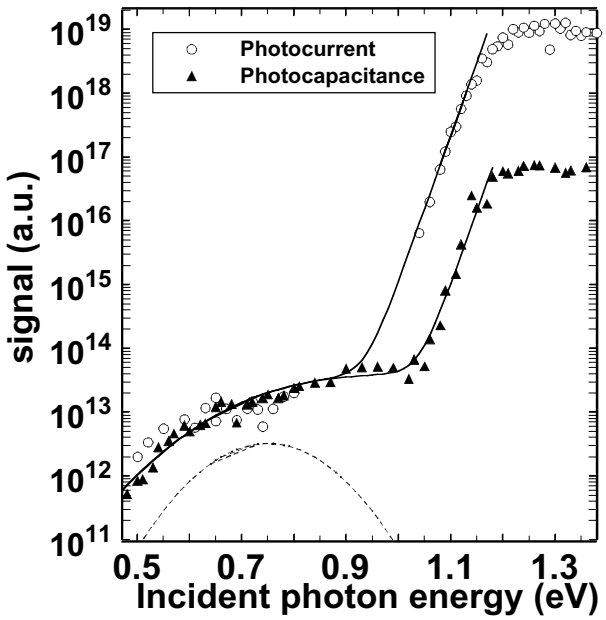

Figure 1. Typical photocapacitance (closed symbols) and photocurrent (open symbols) spectra for a $CuIn_{0.7}Ga_{0.3}Se_2$ device, showing the difference between these spectra caused by minority carrier collection. Fits (solid lines), result from the sum of a Gaussian band of defect states (dotted lines) and an exponential band of tail states.

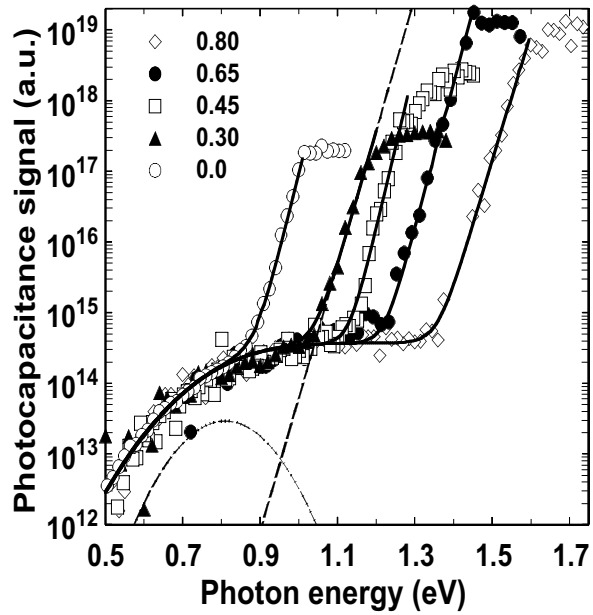

Figure 2. Transient photocapacitance spectra from polycrystalline samples with Ga contents ranging from Ga/(In+Ga) = 0 to 0.8 have been aligned to emphasize the similarity of the deep defect response. Fits (solid lines) are obtained by integrating over a single Gaussian defect band, centered at 0.8 eV, plus an exponential band of tail states.

All of these spectra display two prominent features: (1)˚An exponential dependence at energies extending 0.1 to 0.2˚eV below the optical bandgap energy. This indicates the exponential tailing of states into the gap from the band edges and the characteristic energy of this exponential dependence is called the Urbach energy . The Urbach energies we have determined for the highest efficiency devices produced at IEC lie in the range 16 to 20 meV. (2)˚There is a distinct shoulder that appears at lower optical energies which falls off steeply below about 0.8˚eV. From Fig. 2 we see that its low energy fall-off appears independent of Ga content. By fitting these spectra to a Gaussian shaped defect band plus exponential bandtail (the thin solid lines in Figs. 1 and 2) we have determined that the shoulder arises from an optical transition to an empty defect level 0.8±0.05˚eV above the valence band, with a FWHM of 0.13˚eV for all the samples in this series.[4]

One more important material property can be determined from these measurements. The junction capacitance transient giving rise to the TPC signal reflects the photo-induced change in the charge within the depletion region during the time window. If we induce an optical transition using a photon energy near the optical gap, however, we expect such photons will create both electron and hole carriers in equal numbers. If both types of carriers escape the depletion region then the net charge change is zero, and the capacitance signal would also be zero. The fact that the photocapacitance is not zero in this energy regime reflects the fact that more holes are escaping than electrons. That is, the magnitude of the signal in the bandtail regime is inversely proportional to the relative electron to hole carrier collection fraction, *n/p*. To obtain a quantitative estimate for *n/p* we carry out a complimentary measurement, transient photocurrent (TPI) spectroscopy. In this case the signal is due to the total collected carriers, *n*˚+˚*p*. One such complimentary TPI spectrum is displayed in Fig. 1. The ratio of the TPI to the TPC signals in the bandtail regions is seen to be nearly constant (roughly a factor of 200 in this case). This implies that the collection fraction, *n/p*, is 0.995.

For a second series of samples, deposited with the same Ga content but different substrate temperatures, we have found correlations between some of the parameters determine from our TPC measurements and the device performance. However, these findings are still preliminary.

4. Drive-level Capacitance Profiling

Drive-level capacitance profiling (DLCP) is a variation of the more familiar C-V profiling method to determine carrier densities. It provides a measurement of the density of majority carrier trapping states in the gap both as a function of the thermal energy and of the spatial distance from the barrier. In a DLCP measurement, both a dc offset voltage and an oscillatory drive voltage δV are applied to the device. The amplitude of δV is varied, typically between 10 to over 100 mV. In semiconducting junctions the capacitance not strictly a constant with voltage, but can be expanded as C˚=˚$C_0+C_1\delta V+C_2\delta V^2+$, where C_0 and C_1 are determined by a fit to the data. From these values, the drive level defect density, N_{DL}, can be obtained [5]:

$$N_{DL} = -\frac{C_0^{\,3}}{2q\varepsilon A^2 C_1} = p + \int_{E_{F0}}^{E_V+E_e} g(E,x)dE \qquad (1)$$

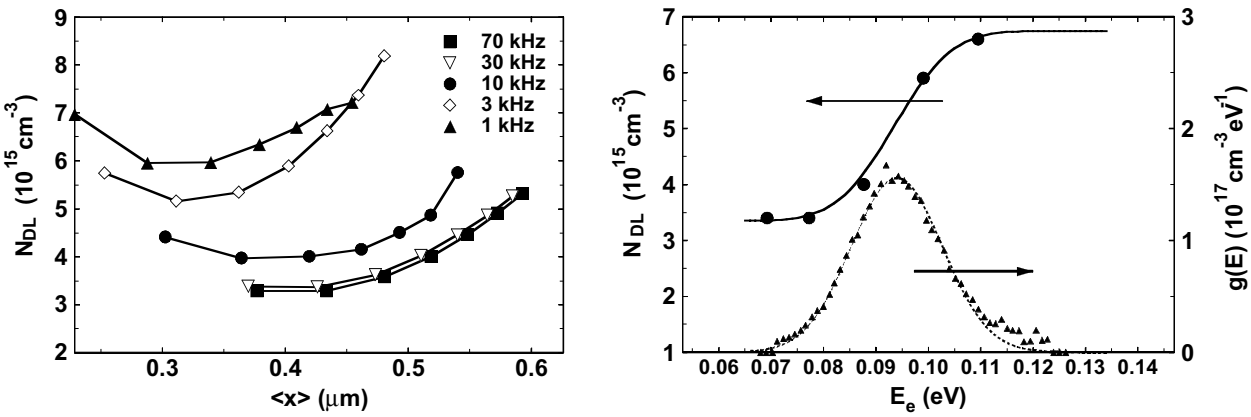

Figure 3. **(a)** Typical DLCP profiles, taken at 110 K for several frequencies as noted in the figure. This device was prepared using T_{ss} = 550 °C. **(b)** Plot of the DLCP value at <*x*> = 0.4μm versus thermal energy E_e, showing more clearly the thermal activation of the defect. E_e was calculated using Eq.2, with $\nu = 5.4\text{x}10^4\ T^2\ \text{s}^{-1}$. The fit to the DLCP response, shown by the solid line, assumes a gaussian shape which corresponds in position and width to the admittance spectroscopy data on the same sample ($\omega dC/d\omega$, triangles, scaled in magnitude to match the DLCP result).

where q is the elemental charge, ε is the material dielectric constant, A is the junction area, E_{F0} is the Fermi energy position in the bulk, and p is the free carrier density in the bulk. This means that N_{DL}, which is obtained by the variation of the junction capacitance with δV is simply related to an integral over the density of states, $g(E,x)$, up to an energy cutoff given by the thermal emission energy E_e determined by the measurement temperature T and (angular) frequency ω; specifically

$$E_e = -k_B T \ln\left(\frac{\omega}{\nu}\right), \qquad (2)$$

where ν is the thermal emission prefactor and typically has temperature dependence $\nu \propto T^2$.

By measuring DLCP for varying values of dc bias, and by varying E_e via changes of temperature or frequency, a spatial and energetic profile of the defect density is obtained. This profile is insensitive to the response from states at or near the interface, except for specific values of dc bias and E_e for which the interface states can dynamically respond to the alternating voltage. This last attribute can be particularly useful in distinguishing the interface from bulk response of defects. Since standard C-V profiling is sensitive to all sources of charge change in the film, it is affected by changes in interface charge that occur during the scan in dc bias, even when the interface defects cannot respond dynamically at the ac frequency. Thus a comparison between C-V and DLCP profiles can distinguish the interface from the bulk response.

Two types of deep defects acting as carrier traps have been frequently reported from admittance measurements of CIGS films. The magnitude of a defect band exhibiting an activation energy, E_a, near 0.3 eV and referred to as N_2 has been correlated with device efficiencies [6]; however, we do not typically observe such a defect response in our devices. A shallower response, with E_a varying between 0.1 and 0.3 eV referred to as N_1 has also been reported [6,7]. Its response energy has been found to vary between devices, and even within the same device after subjecting it to thermal treatment or light soaking [7]. Despite the variations in E_a for different devices, this is thought to be physically the same defect, since the values of E_a and ν_0 are linked by the Meyer-Neldel rule [8]. It has been proposed that this is an interfacial defect acting as an electron trap. We also observe a defect response in our samples with a similar thermal activation energy, between 0.1 and 0.3 eV, which follows the same Meyer-Neldel line as the defect denoted as N_1.

In Fig. 3(a) we show DLCP profiles for a typical device. The value of N_{DL} at low E_e (highest frequencies) indicates the charge density in the depletion region due to the exclusion of the free carriers. As E_e is increased, either by increasing T or decreasing f, the deep defect band begins to respond. At high enough E_e, the entire defect band can respond so that the value of N_{DL} value reaches an asymptotic limit. The difference between N_{DL} measured at high and at low E_e gives the magnitude of the defect band (about $3.5\text{x}10^{15}$ cm^{-3} in this case). This is illustrated more clearly in Fig. 3(b) where the value of N_{DL} at <*x*> = 0.4 μm is plotted versus E_e. According to Eq. 1, the derivative then gives $g(E)$. This is also shown in Fig. 3(b) along with data obtained by taking the logarithmic derivative with respect to frequency of admittance data on the same sample. Whereas previous workers would likely have identified this admittance derived feature as an interface related defect, our DLCP measurements indicate that it must originate from the bulk absorber region of the CIGS. This conclusion is underscored by comparisons with the C-V profiles under the same conditions (not shown).

5. Light-Induced Metastable Defect Creation

A number of previous studies have indicated light-induced changes occur in device properties following long term light exposure. Many of the changes observed have

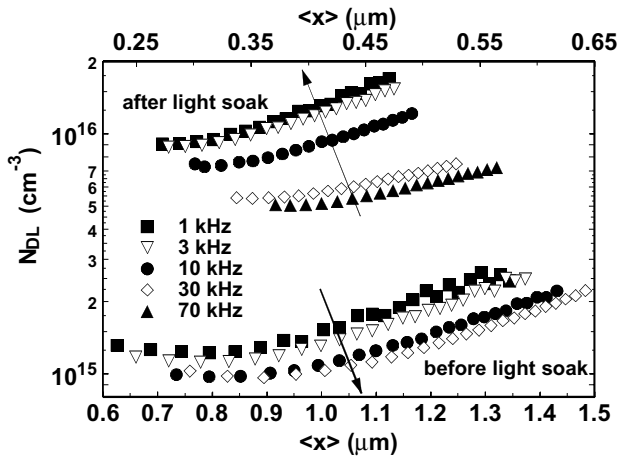

Figure 4. DLCP profiles, before and after light soaking, taken at 135 K. Note that the x-axes differ for the two sets of data. These profiles clearly illustrate a significant increase in carrier density (assumed to dominate the response at high frequencies) and also an increase in the deep trap density. This device was prepared using T_{ss} = 400 °C, but the metastable behavior observed is characteristic of all devices we ve studied.

been attributed to changes in the properties of the junction interface. However, after concluding that N_1 must be a bulk defect in the CIGS absorber itself, we wished to find out whether its properties might also be perturbed by optical exposure. That would confirm a bulk component to the light-induced metastable changes in CIGS.

Our light soaking treatment consisted of exposure to optical excitation at 1064 nm and approximately 100 mW/cm^2, generated by a cw-YAG laser. Unlike most previous studies, our light exposure ensured uniform exposure of the CIGS absorber throughout the depletion region. Samples were typically exposed for 3 hours at 25°C, then immediately cooled in the dark. We subsequently observed significant changes in the average depletion charge density and in the density of deep defects, as illustrated in Fig. 4. These profiles indicate that such changes definitely occur in the bulk region of the CIGS absorber. Indeed, our measurements gave no indication that interface states were introduced, or increased, by this light-soaking treatment.

We also determined the photovoltaic device efficiency of this sample before and after our light treatment using an ELH light source at 100mW/cm^2 intensity. We found a commensurate reduction in conversion efficiency, primarily due to a change in fill factor, from roughly 13% to 11%. Note that the beneficial effects of white light exposure on V_{oc} were not observed for the infared light soaking treatment, despite the observation of increased carrier density. This is perhaps not surprising given the concurrent large increase in the deep defect density. In all devices studied, the metastable changes we observe anneal away in the dark at elevated temperatures, with a time scale of several hours at 50°C.

Previous experiments using red light exposure have also noted an increase in depletion charge density, leading to a decreased depletion width and increased capacitance [9]. This has been attributed to the metastable capture of photogenerated electrons by deep traps in the depletion region. Our observation of an increased free carrier density is not inconsistent with such a mechanism. Alternatively, this result could be due to a real increase in the density of shallow acceptors. The increase in the deep traps, however, cannot be due to such an electron capture mechanism. Moreover, our data indicate that in a given sample the free carrier density and the density of deep traps typically increase by the same amount, suggesting that the mechanisms behind these two types of changes may have a common origin.

6. Conclusions

We have presented a number of experimental results obtained using two methods that are new to the study of the CIGS alloys. The photocapacitance method has allowed to measure Urbach energies, minority carrier collection efficiencies, and has identified a new defect band associated with a 0.8 eV optical transition from the valence band. Although its energy threshold does not change systematically with Ga content, it approaches mid-gap in the higher Ga alloys. This means it would become a much more efficient recombination center in the high Ga alloys. In addition, a band of deep defects has been identified in the bulk region of CIGS films which exhibits metastable changes upon optical exposure. Such light soaking experiments may actually be valuable in identifying which defects act as important recombination centers, if one can correlate changes in their density to changes in device performance.

This work was supported by the National Renewable Energy Laboratory under subcontracts XAD-9-18668-15 (Oregon), and ADJ-1-30630-12 (IEC).

REFERENCES

[1] W. N. Shafarman, R. Klenk, B. E. McCandless, J. Appl Phys. 79 (1996) 7324.

[2] W. N. Shafarman, J. Zhu, Mat. Res Soc. Symp. Proc. 668 (2001) H2.3.

[3] A.V. Gelatos, J.D. Cohen, J.P. Harbison, Appl. Phys. Lett. 49 (1986) 722.

[4] J.T. Heath, J.D. Cohen, W.N. Shafarman, D.X. Liao, and A.A. Rockett, Appl. Phys. Lett. 80 (2002) 4540.

[5] C. E. Michelson, A. V. Gelatos, J. D. Cohen, Appl. Phys. Lett.. 47 (1985) 412.

[6] U. Rau, M. Schmidt, A. Jasenek, G. Ganna, H. W. Schock, Solar Energy Mat. Solar Cells 67 (2001) 137.

[7] R. Herberholz, M. Igalson, and H. W. Schock, J. Appl. Phys 83 (1998) 318.

[8] R. Herberholz, T. Walter, C. M ller, T. Friedlmeier, H. W. Schock, M. Saad, M. Ch. Lux-Steiner, and V. Alberts, Appl. Phys. Lett. 69 (1996) 2888.

[9] U. Rau, et.al. K. Weinert, Q. Nguyet, M. Mamor, G. Hanna, A. Jasenek, H. W. Schock Mat. Res. Symp. Proc. 668 (2001) H9.1